Mapping the magnetic field intensity of light with the nonlinear optical emission of a silicon nanoparticle

Guang-Can Li[1,2], Jin Xiang[1], Yong-Liang Zhang[3], Fu Deng[1], Mingcheng Panmai[1], Weijie Zhuang[1], Sheng Lan[1,], Dangyuan Lei[2,]**

[1] Guangdong Provincial Key Laboratory of Nanophotonic Functional Materials and Devices, School of Information and Optoelectronic Science and Engineering, South China Normal University, 510006 Guangzhou, China. *e-mail: slan@scnu.edu.cn

[2] Department of Material Science and Engineering and Center for Functional Photonics, City University of Hong Kong, 83 Tat. Chee Avenue, Kowloon, SAR, Hong Kong. *e-mail: dangylei@cityu.edu.hk

[3] State Key Laboratory of Superlattices and Microstructures, Institute of Semiconductors, Chinese Academy of Sciences, P.O. Box 912, Beijing, 100083, China.

Content

1. Comparison of the silicon multiphoton luminescence driven by resonant MD and ED excitations

Since both the magnetic and electric excitations in a single Si nanoparticle can generate confined electric near-fields for enhancing the silicon MPL, it is thus crucial to determine which excitation is more efficient. To this end, we simulate the MPL excitation rates of two silicon nanoparticles having either MD or ED resonance at the same wavelength. For simplicity in analysis, we remove the silica substrate present in the experiment. Accordingly, the MD (ED) nanoparticle radius is set as $r_1 = 92$ ($r_2 = 122$ nm) to have a MD (ED) resonance matching the excitation wavelength of 720 nm. Fig. S1c shows spectrally resolved TPL excitation rates calculated for the two silicon nanoparticles, with a plane wave as the excitation field. The results show that the MD nanoparticle

exhibits an excitation rate maximum at the MD resonance whereas the excitation rate of the ED nanoparticle is not peaked at the same wavelength (although its ED mode is resonantly excited). Instead, its excitation rate maximum appears near the MQ resonance, yet with a significantly reduced magnitude with respect to that of the MD nanoparticle. To shed more light on these observations, the two silicon nanoparticles are interrogated with a focused AP beam at the resonance wavelength 720 nm. Fig. S1a schematically illustrates the focal electric field of the AP beam. When a silicon nanoparticle moves from the central site to the beam edge, the electromagnetic excitation it experiences transits from a pure magnetic type to a pure electric one. Fig. S1b displays the evolving electric near-field intensity distributions simulated for the two silicon nanoparticles: the field intensities of the MD nanoparticle are found to be the strongest at the beam center site where its MD mode is resonantly excited, whereas that for the ED particle only becomes significant when the particle enters the outer ring-shaped area where electric fields are non-vanishing. Importantly, compared to the ED excitation, the MD excitation induced electric fields are more tightly confined in the MD particle volume, thus leading to higher TPL excitation rates as observed at the MD resonance. In this regard, the MD nanoparticle enables an efficient nanoprobe to map magnetic fields at optical frequencies. As shown in Fig. S1d, the position dependent TPL excitation rate of the MD nanoparticle well retrieves the magnetic field distribution of a focused AP beam. In contrast, scanning an ED nanoparticle through the focal fields is found to map the electric field distribution, yet with much lower efficiency.

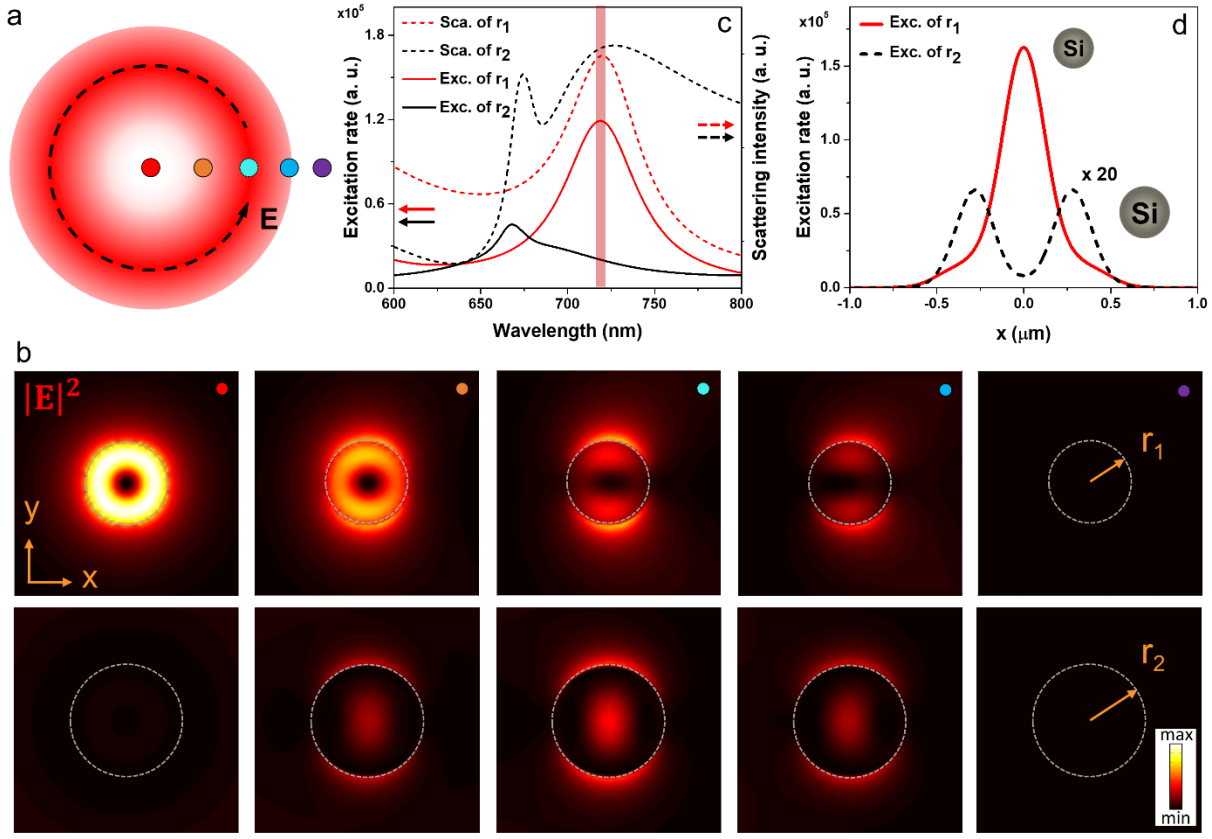

Figure S1 Comparison of MPL excitation rates for silicon nanoparticles pumped at the MD and ED resonance wavelengths. (a) A schematic illustrating the electric field intensity profile of a focused AP beam, with several sites marked for the results presented in (b). (b) Simulated near-field distributions for a silicon nanosphere with a MD (upper panel, smaller particle size, $r_1 = 92$ nm) or an ED (bottom panel, larger particle size, $r_2 = 122$ nm) resonance matching the excitation wavelength of 720 nm. For simplification, the MD and ED nanoparticles are immersed in air in simulation. All the field distributions are rendered on the same intensity scale for direct comparison. (c) Wavelength-dependent MPL excitation rates calculated for the two silicon nanoparticles of 92 nm (solid red line) and 122 nm (solid black line) in radius (the same as (b)). Corresponding scattering spectra (dashed lines) are also presented for reference. (d) Simulated line profiles of MPL excitation rate for the two silicon nanoparticles as in (b) and (c) scanned by an AP beam. The 92 nm particle experiences resonant magnetic excitation while the 122 nm particle experiences resonant electric excitation at the pump wavelength.

2. Details about the scalar approximation taken in the main text

In the main text, the formula linking the external magnetic field stimuli and the inner-particle fields (copied in below, Eq. S1) and the one used to evaluate the silicon photoluminescence (Eq. S2) both contain an integral term defined on the nanoparticle volume.

$$\alpha_m \vec{H}_0(\vec{r}) = \frac{i\omega_0(\epsilon_s - \epsilon_0)}{2}\int_V \overrightarrow{r'} \times \overrightarrow{E'}(\overrightarrow{r'})dV \quad (S1)$$

$$I_{\mathrm{TPL}}(\vec{r}) \propto \int_V \left|\overrightarrow{E'}(\overrightarrow{r'})\right|^4 dV \quad (S2)$$

When deriving the explicit form relating the single nanoparticle photoluminescence with the external magnetic stimuli, it is crucial to work out the analytical solution of these integrals. To this end, we took the following approximations: (1) the integral results are dominated by the torque-shaped volume (V_T) near the equatorial plane (refer to the inset of Fig. S2), and (2) the circulating electric field witin the thin torque volume varies slowly in magntude and thus can be assumed to be cosntant (*i.e*. the scalar approaximation). In other words, the averaged electric field magnitude can reprsent this constant, defined as $\langle\left|\overrightarrow{E'}\right|\rangle = \frac{1}{V_\mathrm{T}}\int_{V_\mathrm{T}}\left|\overrightarrow{E'}\right|dV$. These approximations are supported by the simulated field distribution at the MD resonance (as shown in Fig. S2) and the high TPL contribtion factor of the equatorial domain V_T, as defined by

$$\eta = \frac{\int_{V_\mathrm{T}}\left|\overrightarrow{E'}(\overrightarrow{r'})\right|^4 dV}{\int_V \left|\overrightarrow{E'}(\overrightarrow{r'})\right|^4 dV} \approx 92.7\% \quad (S3)$$

Because of the azimuthally polarized electric fields in V_T, the intergral in Eq. S1 can be simplified as

$$\int_V \overrightarrow{r'} \times \overrightarrow{E'}(\overrightarrow{r'})dV = \vec{e}\int_V \left|\overrightarrow{E'}(\overrightarrow{r'})\right|dV \approx \vec{e}\int_{V_\mathrm{T}} \left|\overrightarrow{E'}(\overrightarrow{r'})\right|dV = \vec{e}V_\mathrm{T}\langle\left|\overrightarrow{E'}\right|\rangle \quad (S4)$$

The Eq. (S1) can thus be re-written as

$$\alpha_m \vec{H}_0(\vec{r}) \approx \frac{i\omega_0(\epsilon_\mathrm{s}-\epsilon_0)}{2} V_\mathrm{T}\langle\left|\overrightarrow{E'}\right|\rangle\vec{e} \quad (S5)$$

In the same way, we have

$$I_\mathrm{TPL}(r) \propto \int_V \left|\overrightarrow{E'}(\overrightarrow{r'})\right|^4 dV \approx V_\mathrm{T}\langle\left|\overrightarrow{E'}\right|^4\rangle \quad (S6)$$

Since the electric field magnitudes vary slowly in V_T, we can assume:

$$\langle\left|\overrightarrow{E'}\right|^4\rangle \approx \langle\left|\overrightarrow{E'}\right|\rangle^4 \quad (S7)$$

.

From the above three equations, we can formularize the photoluminescence intensity of a single silicon nanoparticle as a function of the in-site magnetic field, formulated as

$$I_\mathrm{PL}(r) \propto |H_0(r)|^4 \quad (S8)$$

This explicit expression can be validated by comparing the numerical result of Eq. S2, calculated for a single silicon nanoparticle scanning a focused light beam, and the calculated $|H_0(r)|^4$ profile (according to Eq. S8) of the same beam, which show good agreement as shown in Figs. 3e and 4c in the main text, confirming the rational and validity of the above approximations.

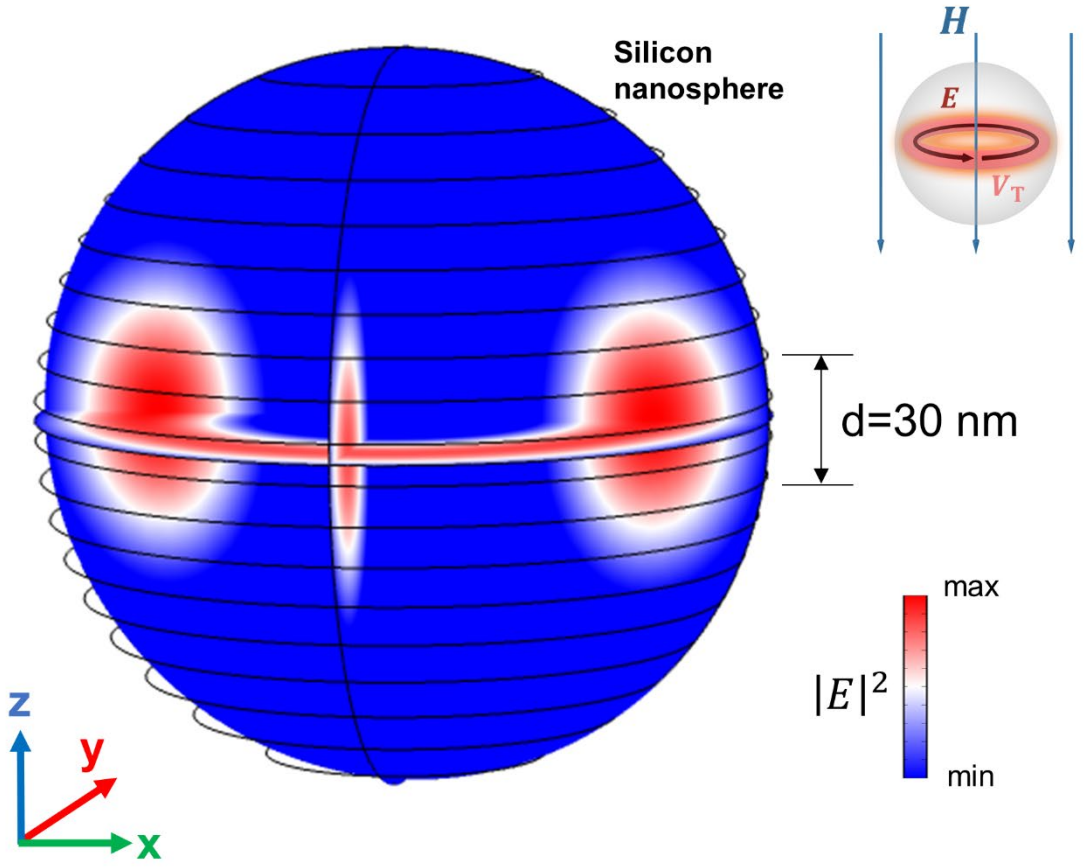

Figure S2 Simulated electric field distribution at the MD resonance wavelength (720 nm) of a silicon nanosphere (185 nm in diameter). In the simulation, the excitation field is a plane wave incident along the *x* direction, with the magnetic field component polarized along the *z* axis.

3. Excitation properties of photoluminescence from silicon nanoparticles

In Fig. S3a, a rapid decrease in the MPL intensity is observed when the excitation wavelength deviates from the MD resonance of a silicon nanoparticle, indicating an efficient MD resonance enhanced photoluminescence process. For the silicon nanoparticles having a MD resonance at ~720 nm, we observed a linear relationship between the MPL intensity and the excitation energy in the logarithmic coordinate (Fig. S3b), suggesting that the MPL emission originates from two-

photon-absorption (TPA) induced luminescence. Considering the large silicon bandgap at the Γ point (~3.4 eV), higher-order absorption induced photoluminescence may occur at longer wavelengths (beyond 720 nm). For example, three-photon absorption induced luminescence from larger silicon nanoparticles can occur when their MD modes are resonantly excited in the near-infrared wavelength region (see Ref. 23 in the main text).

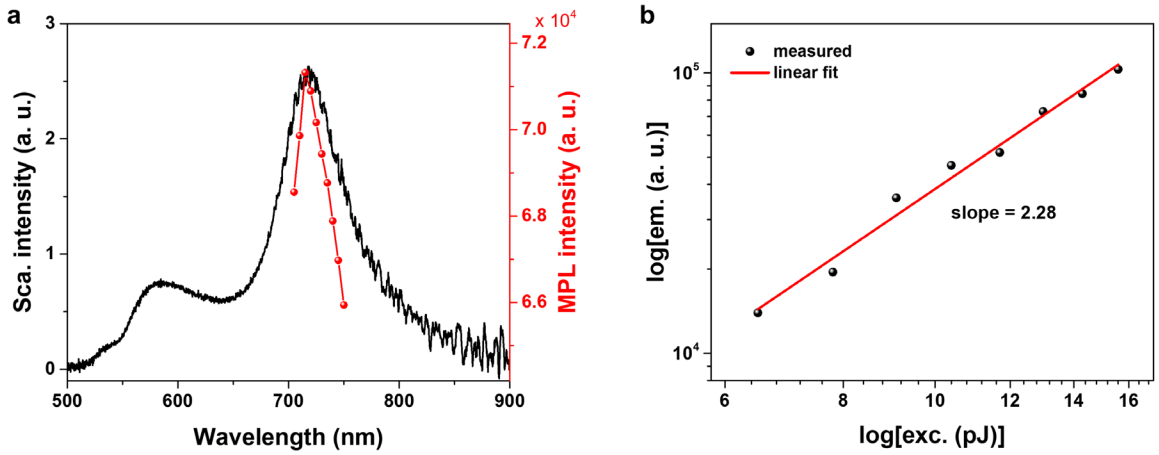

Figure S3 (a) Measured MPL excitation (red) and scattering (black) spectra for a single spherical silicon nanoparticle with a MD resonance at ~720 nm. (b) Log-log plot of excitation energy dependent MPL intensities. The femtosecond laser excitation wavelength is 720 nm and the collection band for evaluating MPL intensities is 500-600 nm.

4. Effect of the silicon nanoparticle size on field distribution mappings

In our experiment, the magnetic field distributions mapped by different silicon nanoparticles (refer to Fig. 3c) in a single frame show slight differences in pattern size. This is mainly caused by the inhomogeneity in particle size. Specifically, when the pattens of individual nanoparticles mapped in the same frame are rendered on the same intensity scale (refere to the reference line in Fig. S4a), the nanoaprticles with MD resonances closer to the laser wavelenght seem to be brighter and larger than the others in the same image. Nevertheless, the normalized TPL excitation intesnity profiles of the silicon nanopartices with slight size differences show no significant devations from each other (see Fig. S4b). On the other hand, one may imagine that considerabl electric excitation

could occur in silicon nanoparticles with MD resonances singificantly red-shifted from the laser wavelength. Mapping the focal fields with such nanoprobes would thus give rise to electric-dressed magnetic field distribtuion (indicated by the arrow in Fig. S4b). Fortunately, the TPL excitation rate under this condition is typically low and thus the electric effect is marginal in the overall result.

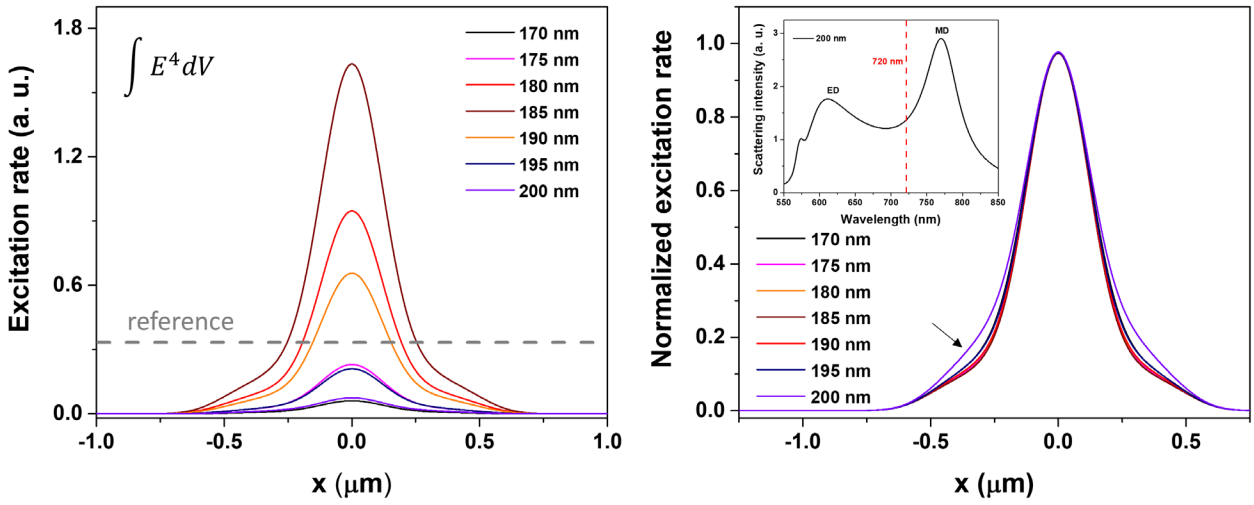

Figure S4 Left panel: Simulated line profiles of particle size dependent TPL excitation rates for single silicon nanospheres scanning through the focal plane of an AP beam. The AP laser wavelength is fixed at 720 nm and the particle size varies from 170 nm to 200 nm in a step of 5 nm. Right panel: The same data as in the left panel are normalized to better visualize the negligible electric excitation contribution in the silicon nanoparticles with MD resonances significantly deviated from the laser excitation wavelength. The slight profile deviation indicated by the arrow is caused by concurrent electric excitation, which becomes significant for larger particles. For reference, the inset shows the scattering spectrum of a 200 nm diameter silicon nanosphere in air.

In addition, scanned TPL images of single silicon nanoparticles can show different intensity patterns at different excitation wavelengths. For example, an air-immersed silicon nanosphere of 185 nm diameter shows a MD resonance at 720 nm and an ED resonance at a shorter wavelength (~ 600 nm). When the excitation wavelength varies from 755 nm to 575 nm, the siliicon nanoparticle experiences a continuous transition from magneitc to electric excitation. This is manifested unambigously by the simulated line profiles of TPL excitation rates for the silicon nanosphere at different excitation wavelengths as shown in Fig. S5. At short wavlengths (i.e. 575

nm, 605 nm, and 635 nm), each line profile displays a clear doublet shape, indicating that the nanoparticle actually maps the electric field distribution of the focused AP beam. At longer wavelenghs (i.e. at or above the MD wavelength, 725 nm and 755 nm), a singlet appears in each line profile, corresponding to the TPL mapping of the mangenic field distrbution. At intermediate wavelenghs (665 nm and 695 nm, for example), the TPL excitation rate line profiles take on a mixed electric and magnetic field character, implying the co-existence of electric and magnetic excitations. Finally, it is found that the TPL excitaiton is most efficient at the MD wavelength (i.e. at 725 nm), consistent with the analytial results shown in Fig. S1. To map exlusively the magnetic field component of light, it is thus preferred to select a silicon nanoprobe with the MD resonance at the excitation wavelength.

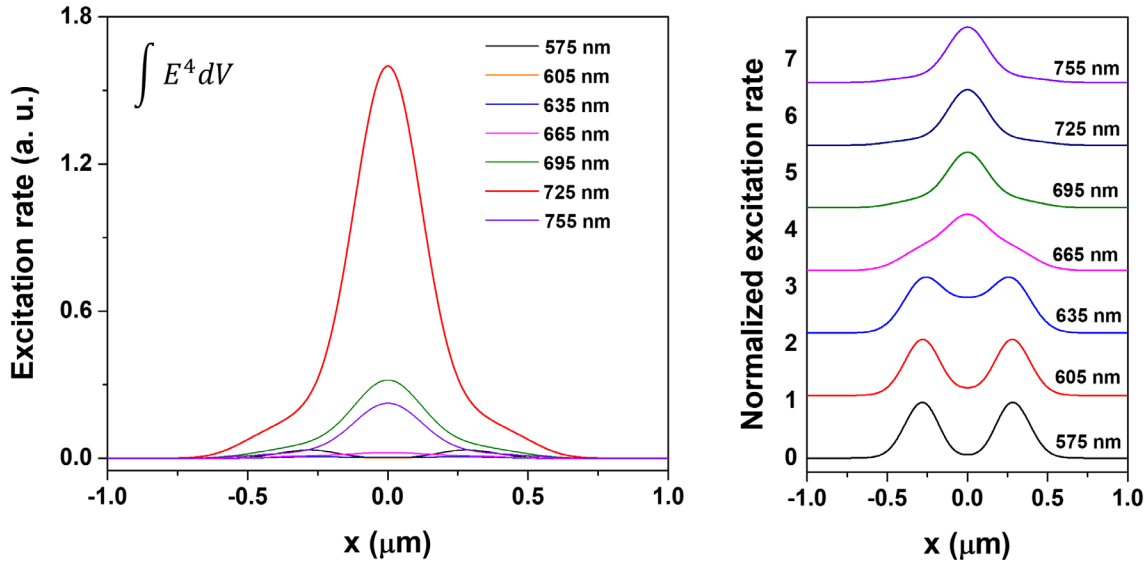

Figure S5 Left panel: Excitation wavelength dependent TPL excitation rate profiles simulated for a silicon nanosphere scanning through the focal plane of an AP beam. The nanoparticle exhibits a MD resonance at 720 nm, and its two-photon excitation rate is evaluated by the integral, $\int E^4 dV$, with the integration domain going over the particle volume. In the simulation, the numerical aperture for collecting TPL signals is set to be 0.95. Right panel: For clarity, the same data in the left panel are normalized and shown in an offset manner in the right panel.

5. Multiphoton luminescence responses of gold nanoparticles

Gold nanospheres used in this study were purschased from Nanoseedz Ltd., with a nominal diamter of ~100 nm. The dark-field scattering spectrum of such a single gold nanoparticle on silica substrate shows a prominent dipolar plasmon resoannce at ~560 nm, implying a strong interation between the particle and the electric field component of the incident light (Fig. S6a). At the femtosecond laser wavelenth 720 nm, the mode excited in the gold nanoparticle has a dipolar character. Because of the non-resoant excitation condition at this wavelength, the MPL signal of a single gold nanoparticle is relatively weak with respect to its silicon counterpart and, in our experiment, its spectral characters can be resolved only with a sensitive PMT detector. Note that the MPL spectrum of single silicon nanoparticles in Fig. 2b is recored with a cooled CCD camera that fails to detect the TPL singnal from a single gold nanospshere.

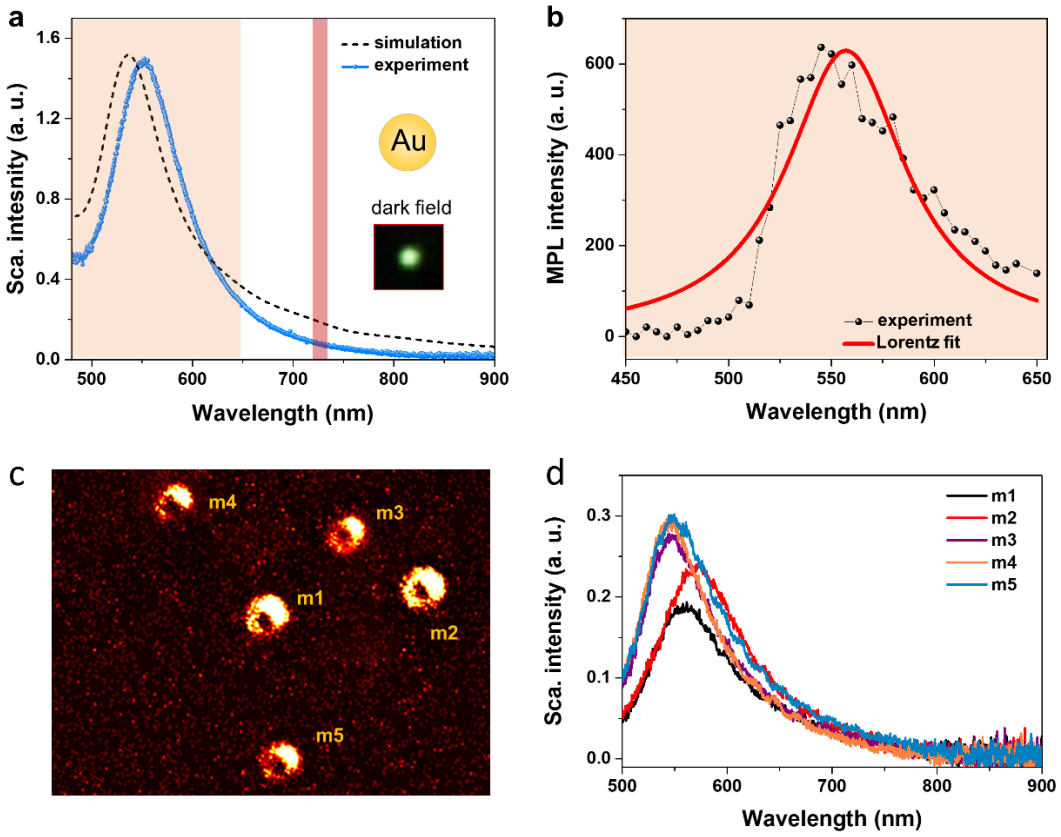

Figure S6 (a) A representative scattering spectrum (solid green line) of a single ~100 nm gold nanosphere, with its dark-field optical image shown in the inset. For simplicity, in simulation the nanoparticle is embedded in air. This simplification results in a blue shift in the plasmon resonance wavelength (dashed black line) with respect to its counterpart on a silica substrate. (b) Measured MPL spectrum (black) for the gold nanosphere in (a). The pumping laser wavelength is 720 nm, corresponding to a non-resonant excitation condition for the gold nanoparticle. A rotating grating inside the monochromator together with a sensitive PMT detector is used to measure the weak spectral response, with an acquisition step of 5 nm. The red curve is a Lorentz fit to the experimental data. (c) TPL image obtained by scanning Au nanoparticles through the focal plane of a focused AP beam (copied from Fig. 3d in main text). (d) Measured scattering spectra of the Au nanoparticles marked in (c). All the Au nanoparticles exhibit nearly the same plasmon modes at ~550 nm.

Owing to the large dissipation loss, the magnetic response of a single gold nanoparticle is negligible with respect to its electric response. This is unambiguously revealed by the near-field intensity disribution of the gold nanoparticle scanning through a focused AP beam. As shown in Fig. S7, when the particle is resident at the focal site where electric field is non-vanishing, the electric field driven localized surface plasmon generates a strong near-field hot spot. When moving to the central site where electric field is vanished, the near-field intensity pattern of the nanoparticle becomes totally invisible, though the magnetic field reaches its maximial intensity at this site.

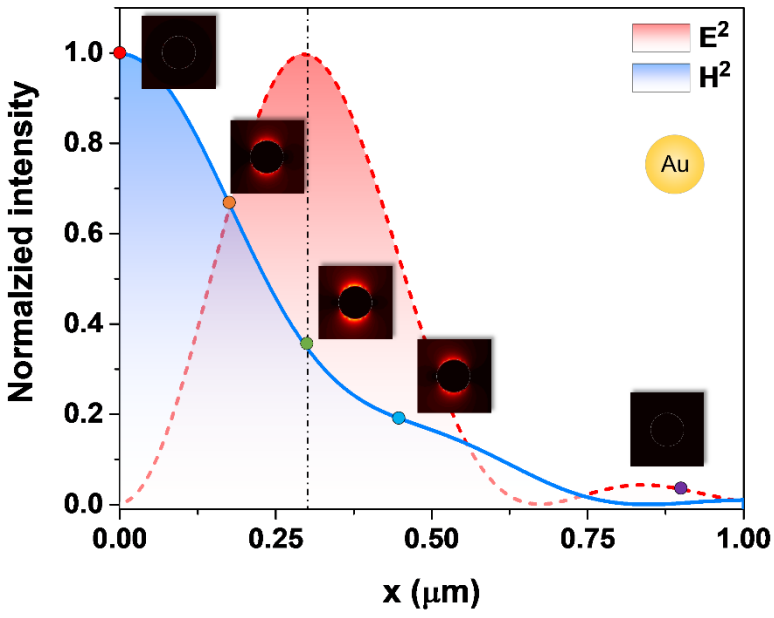

Figure S7 Electric-field intensity distribution of a gold nanosphere residing at different positions in the focal plane of a focused AP beam. The zero position ($x = 0$) corresponds to the focus center where electric field is vanishing. All the near-field intensity patterns are rendered on the same intensity scale.

6. Mapping the intensity distributions of circulating magnetic fields

In this part, we compare the field mapping results of a focused radially-polarized (RP) beam using single gold and silicon nanospheres, respectively. Fig. S8a shows that the gold nanoparticle map appears as a solid circular spot, consistent with its electric field intensity distribution in Fig. S8b. In contrast, the silicon nanoparticle map shows a doughnut-shaped pattern, agreeing well with the calculated magnetic field intensity distribution in Fig. S8d. Note that the magnetic field vector in Fig. S8d exhibits circulating orientation, confirming the polarization-insensitive character of the silicon-based magnetic field nanoprobe.

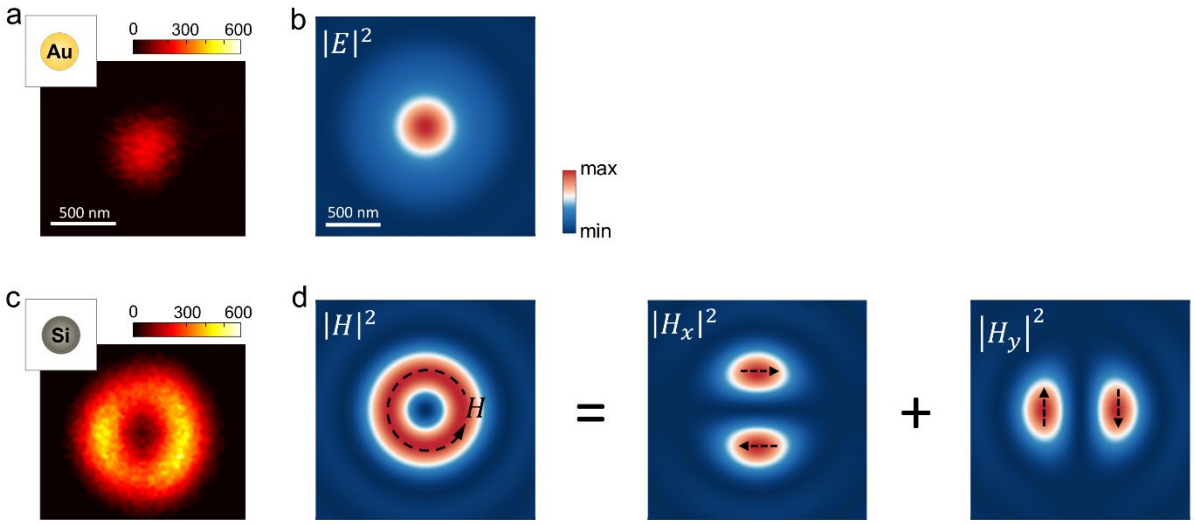

Figure S8 Field intensity distributions of a focused radially-polarized beam mapped respectively by gold and silicon nanoparticles. (a) The focal intensity pattern of the beam mapped by a single gold nanoparticle (~100 nm in diameter). (b) Calculated electric field intensity distribution of the beam in the focal plane. (c) The focal intensity pattern of the beam mapped by a single silicon nanoparticle (~180 nm in diameter). The pattern is rendered on the same intensity scale as (a). (d) The magnetic field intensity distribution of the beam in the focal plane. The local magnetic field in the left panel shows an azimuthally-polarized vector character and thus represents an example field with concurrent multipole magnetic field components as shown by the decomposed field distributions (right panels).

7. Spectral separation between the ED and MD resonances of silicon nanoparticles

The magnetic responses of naturally occurring materials are typically limited to specific frequencies that are determined by chemical composition and crystal structure, and their magnetic transitions are often in close spectral proximity to the electric counterparts. In contrast, the MD and ED resonances of a high-index silicon nanoparticle can be flexibly tuned over a wide spectral range by simply changing the particle size (see Fig. S9a) and are well separated from each other, which significantly reduces the crosstalk effect between the two resonances. For example, the spectral separation between the ED and MD resonances of a silicon nanosphere is found to be typically > 100 nm (see Fig. S9b) and increases with the sphere diameter, largely exceeding that between the electric and magnetic transitions in rare earth ions (typically < 10 nm). Note that, to explore the weak magnetic transitions in rare earth ions, the samples are usually placed in cryogenic environment to suppress the spectrally adjacent electric transitions.

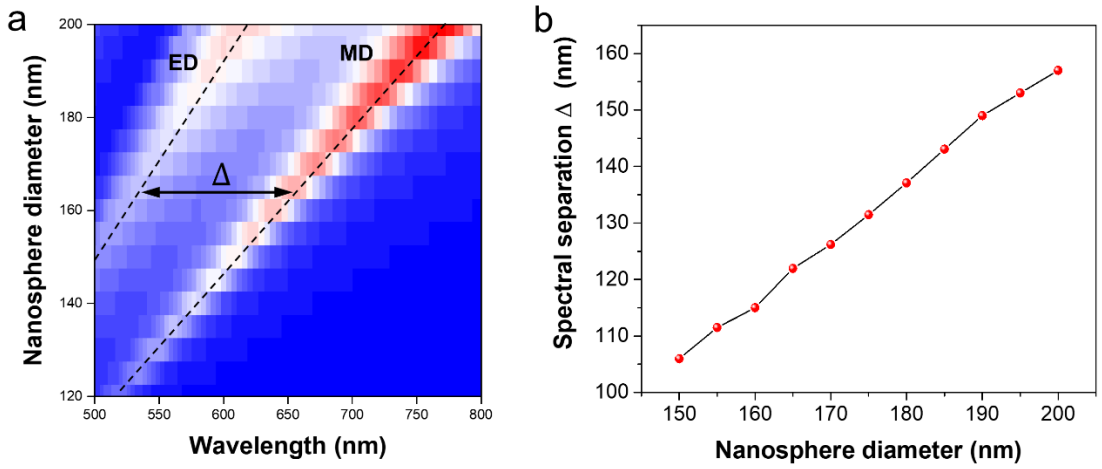

Figure S9 (a) Contour plot of the scattering intensity of silicon nanospheres (in air) as functions of sphere diameter and light wavelength. (b) Spectral separation between the ED and MD resonances of silicon nanospheres as a function of sphere diameter.

8. Experimental setup

Far-field scattering spectra of single Si nanoparticles were measured using an inverted fluorescence microscope (Observer A1, Zeiss) equipped with a transmissive-type dark-field illuminator. An oil-immersed 100×objective (Plan-NEOFWAR, Zeiss) with tunable numerical aperture (NA, 0.7-1.3) were used to collect the scattered light of a single Si nanoparticle and then direct it to a monochromator (SR500, Andor) equipped with a cooled CCD camera (DU970N, Andor) for spectral analysis. The MPL spectrum of single Si nanoparticles was also measured on the same microscope platform, with an external Ti:sapphire femtosecond laser (Mira 900S, Coherent) as the excitation source.

Based on the above MPL spectroscopy platform, the setup for mapping the magnetic field distributions of highly focused laser beams is constructed, as shown in Fig. S10. A Ti:sapphire femtosecond oscillator is employed to generate pulsed laser with a time duration of ~130 fs and a repetition rate of 76 MHz. Before entering the microscope, the laser beam is coupled to a single-mode fiber with a microscopic objective (see the inset in Fig. S10). The laser from the output end is then collimated with a plano-convex lens, generating a beam with an optimized Gaussian intensity profile. A Glan prism is used to polarize the beam. An azimuthally polarized beam can be obtained by passing the linearly polarized Gaussian beam through a radial polarization converter (working wavelength 720 nm, customized from ARCoptix, Inc.). An oil immersed objective is used to focus the tailored laser beam onto the sample plane. The sample is positioned in the focal plane and mounted onto a piezo stage (P563.3CD, Phyisik Instruments) that can drive silica-supported nanoparticles moving through the focal fields. MPL signals from single

nanoparticles are collected by the same objective and then separated from the excitation laser by passing through a dichroic mirror and subsequently a short-pass filter. The spectrometer system, consisting of a monochromator equipped with a CCD camera and a PMT detector, is used to spectrally resolve the TPL signals and select the wavelength band for scanning images. The TPL maps are formed by raster scanning the sample through the focused laser spot and simultaneously recording the signal intensity pixel by pixel. To avoid potential laser-induced photodamage to the particles in the scanning process, the laser power was restricted to below 1 mW and the laser dwelling time at each pixel was 0.2 sec.

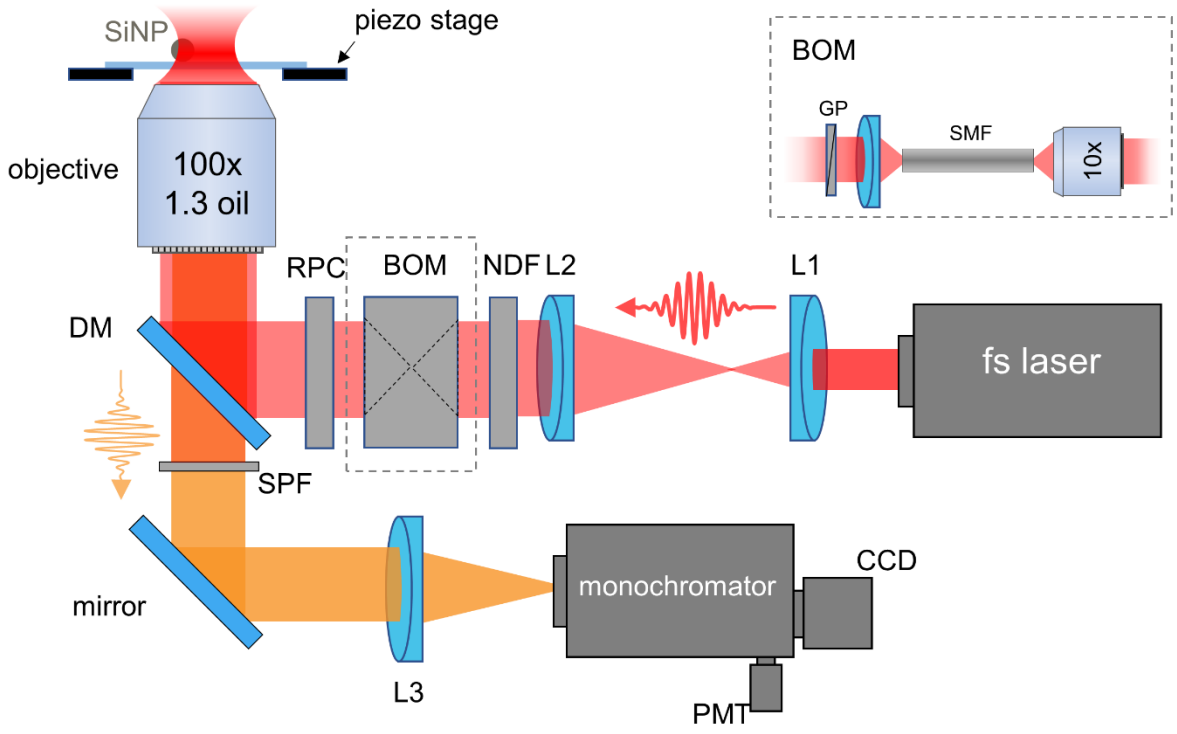

Figure S10 Experimental setup for mapping the magnetic field distributions of tightly focused laser beams. The main optical components include a high NA objective, dichroic mirror (DM), radial polarization converter (RPC), neutral density filter (NDF) with adjustable attenuation amplitude, short-pass filter (SPF) and several lenses (L1-L3). The beam optimization module (BOM), consisting of a single-mode fiber (SMF), a Glan prism (GP) and two lenses, is used to improve the quality of the raw Gaussian laser beam from the Ti:sapphire laser source.

9. Evaluation of the substrate effects on the silicon nanoprobes

For simplicity in analysis, we illustrated the working principle of our silicon nanoprobe by considering a nanosphere suspended in air. In experiments, however, the silicon nanosphere was supported by a silica substrate. In this section, we will evaluate the effects of a silica substrate on the performance of the silicon nanoprobes based on numerical simulation. We first compare the scattering spectrum of a silicon nanosphere (with a diameter 185 nm) supported by a silica substrate with that suspended in air. As shown in Fig. S11a and b, the introduction of a silica substrate does not change the resonant wavelengths of the ED and MD resonances of the Si nanosphere. However, the amplitudes of the ED and MD resonances are modified to some extent, due mainly to the interaction between the reflection induced by the substrate and the direct scattering of the nanosphere. In addition, a magnetoelectric coupling effect is observed for the Si nanosphere located on the silica substrate, as indicated by the red arrow in Fig. S11b. It implies an increased electric response at the MD resonance, which has been studied previously[1,2]. It was attributed to the substrate-induced interaction between the ED and MD modes. In this case, we didn't observe protuberance or valley at the ED resonance, due mainly to the relatively low refractive index of silica (n~1.5). Apparently, such magnetoelectric coupling effect induced by the substrate is not desirable for a perfect electric (magnetic) probe.

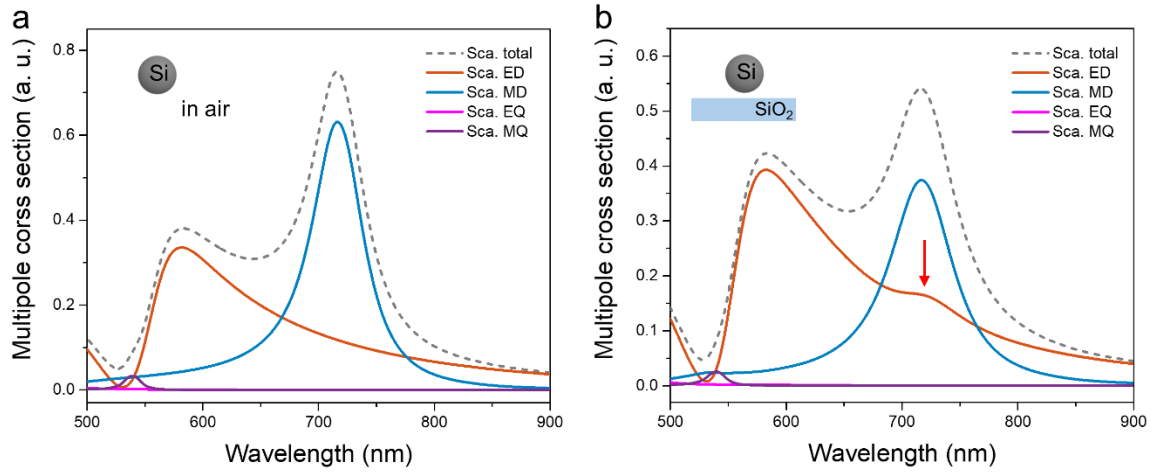

Figure S11 Comparison of the scattering spectra (dashed curves) of silicon nanoparticles (with a diameter 185 nm) suspended in air (a) and located on a silica substrate (b). In each case, the scattering spectrum has been decomposed into the contributions of various Mie resonances (i.e., ED, MD, EQ, and MQ). For the nanoparticle on the silica

substrate, the particle-substrate gap is set to be 2 nm. In the numerical simulations, a plane wave was used as the excitation source to excite the Si nanoparticles.

In this work, the physical mechanism used for probing the magnetic field of light relies on the detection of the two-photon-induced luminescence from single silicon nanoparticles, rather than their scattering which was usually used in previous studies (refer to Ref. 3, 18 and 19). When the scattering of a nanoparticle was employed to probe the magnetic field of light, the existence of a substrate may significantly modify the far-field scattering properties of the nanoparticle probes through the background reflection. In our case, the TPL emitted by a Si nanoparticle was employed as the optical signal for probing the magnetic field of light. It is noticed that the electric field at the MD resonance is mainly localized inside the Si nanoparticle while that at the ED resonance is mainly distributed outside (see Fig. 1b and 1c). Such distinct field distributions suggest that the TPL of the Si nanoparticle excited at the MD resonance comes predominantly from the MD resonance while the contribution of the ED resonance is negligible. As stated in the main text (Eq. xx), the excitation efficiency of the TPL can be evaluated by calculating the integral $\int E^4 dV$ over the nanoparticle volume. In Fig. S12a, we present the calculated wavelength-dependent TPL excitation efficiency for a Si nanosphere in air. It can be seen that the TPL excitation efficiency at the ED resonance is much lower than that at the MD resonance owing to the difference in the electric field distribution. As a result, the ED resonance is not resolved in the spectrum of $\int E^4 dV$, implying its contribution of the ED resonance to the TPL is negligible. This conclusion holds true for the Si nanoparticle located on the silica substrate (see Fig. S12b), where the substrate-induced magnetoelectric coupling effect is only clearly revealed (see Fig. S11b). Therefore, we can conclude that the influence of the silica substrate on the performance of the Si nanoprobe can be neglected. To further confirm this, we compare the field mapping results obtained without and with the silica substrate, as shown in Fig. S12c and d. It can be seen that the simulated TPL intensity profile follows exactly the calculated $|H|^4$ lineshape in both cases, indicating that a Si nanoparticle supported by a silica substrate acts as a nanoprobe for the magnetic field of light. However, other substrates with large dielectric constants, such as semiconductors and metals, may strongly interact with the Si nanoparticle and generate complicated optical resonances which may deteriorate the performance or even disable the magnetic field nanoprobe. In addition, the presence of the substrate can modify the emission properties of the Si nanoparticles.

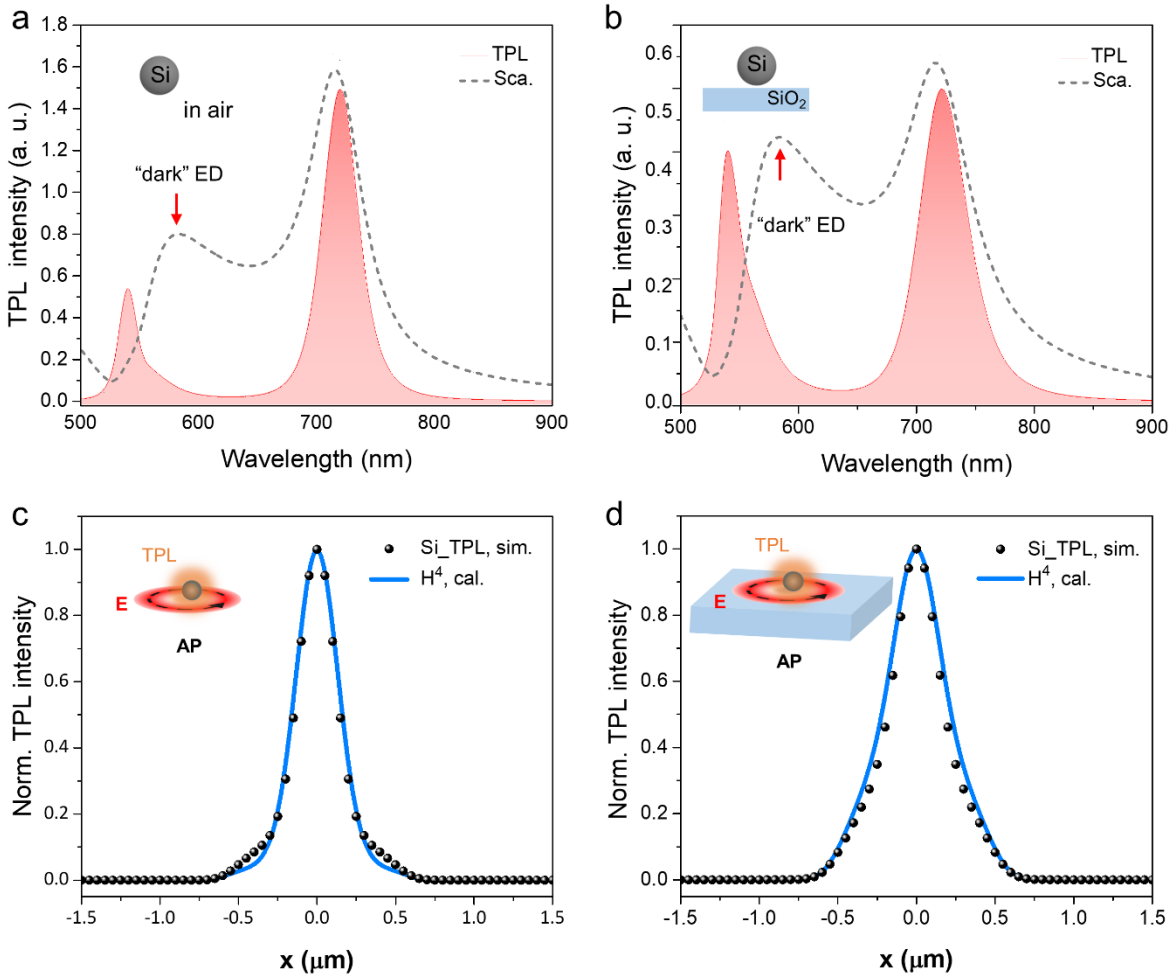

Figure S12 (a, b) Comparison of the TPL excitation efficiency spectra of single Si nanoparticles in air (a) and on glass substrate (b). The corresponding scattering spectra are also provided for reference. Note the pronounced ED resonance in the scattering spectra are vanished in the TPL excitation efficiency spectra, due mainly to the poor spatial overlapping of induced electric near-fields and the nanoparticle volume. (c, d) Comparison of the TPL mapping results of a focused AP beam using a Si nanoparticle probe in air (c) and on glass substrate (d). The geometry parameters of the nanoprobe construct are identical to that used in Fig. S11. Note the presence of the glass substrate slightly expands the intensity profile of the focused beam, compared to that in air.

10. References

(1) Markovich, D. L.; Ginzburg, P.; Samusev, A. K.; Belov, P. A.; Zayats, A. V. Magnetic Dipole Radiation Tailored by Substrates: Numerical Investigation. *Opt. Express* **2014**, *22* (9), 10693.

(2) Miroshnichenko, A. E.; Evlyukhin, A. B.; Kivshar, Y. S.; Chichkov, B. N. Substrate-Induced Resonant Magnetoelectric Effects for Dielectric Nanoparticles. *ACS Photonics* **2015**, *2* (10), 1423–1428.